Application of Radial Basis Neural Networks in Fault Diagnosis of Synchronous Generator

H. Yaghobi[1] H. Rajabi Mashhadi[2] K. Ansari[3]

[1] Assistant Professor, Faculty of Electrical Engineering, Semnan University, Semnan, Iran
yaghobi@profs.semnan.ac.ir
[2] Professor, Department of Electrical Engineering, Ferdowsi University of Mashhad, Mashhad, Iran
h_mashhadi@um.ac.ir
[3] Assistant Professor, Department of Electrical Engineering, Ferdowsi University of Mashhad, Mashhad, Iran
ansari@um.ac.ir

Abstract :

This paper presents the application of radial basis neural networks to the development of a novel method for the condition monitoring and fault diagnosis of synchronous generators. In the proposed scheme, flux linkage analysis is used to reach a decision. Probabilistic neural network (PNN) and discrete wavelet transform (DWT) are used in design of fault diagnosis system. PNN as main part of this fault diagnosis system and DWT are combined effectively to construct the classifier. The PNN is trained by features extracted from the magnetic flux linkage data through the discrete Meyer wavelet transform. Magnetic flux linkage data is provided by a FEM (Finite Element Method) simulation of a real synchronous generator and estimated by generalized regression neural network (GRNN). Then PNN is tested with experimental data, derived from a 4-pole, 380V, 1500 rpm, 50 Hz, 50 KVA, 3-phase salient-pole synchronous generator.

Keywords: Radial basis neural network, Synchronous generator, Fault diagnosis, Linkage flux analysis.

Submission date: 01 Jan. 2012

Conditional acceptance date: 25 Sep. 2012

Acceptance date: 16Jan. 2013

Corresponding author: Hamid Yaghobi

Corresponding author's address: Elec. Eng. Faculty., Semnan University, Semnan, Iran

1. Introduction

Fault detection and diagnosis of electrical machines are of particular importance in industry and have moved in recent years from conventional techniques to Artificial Intelligence (AI) techniques [1]. ANNs imitate the human brain formation, which consists of simple arithmetic units connected in complex layer architecture. They have the ability of nonlinear mapping, parallel processing and learning [2]. These features make them ideally suited for providing a high accuracy in fault detection under a wide variety of different systems and fault conditions. The AI techniques have numerous advantages over conventional fault diagnostic approaches [1]. Besides giving better performance, these techniques are easy to be extended and modified. These can be adaptive by incorporating new data or information. AI techniques are now being increasingly used for condition monitoring and fault detection of electrical machines [3, 4]. Also, several papers have presented different methodologies based on the inclusion of expert systems to classification of power quality disturbances, transformer faults and significant events with probabilistic neural network [5-12].

On the other hand, the stator's internal short circuit current in the synchronous generator may be several times larger than its terminal short circuit current. When an inter-turn short circuit occurs, the shorted turn will act as the secondary winding of an autotransformer. Consequently, a very large circulating current will flow in the faulted turn. This circulating current creates excessive heat and high magnetic forces in the machine [13].Therefore, it is very important to have a careful analysis of the internal faults in synchronous generators to increase their useful life and reliability. Hence, this paper describes the design and implementation of an artificial neural networks-based fault locator for salient-pole synchronous generator. This technique uses radial basis function (RBF) neural networks for locating internal faults in salient-pole synchronous generator. This locator utilizes magnetic flux linkage waveforms of the fault data. These values are stored as waveform samples by a designed data recorder. Then the faulted waveform samples are transferred to a standard personal computer (PC). The incoming data after processing in PC is fed to the trained ANNs for locating internal faults. The RBF networks are trained with data under a variety of fault conditions and used for fault location. The advantage of this method is the best understanding of the local phenomena (magnetic flux linkage) and high accuracy of detection.

2. Radial Basis Neural Network and Wavelet Analysis

2.1. Radial Basis Function Neural Networks (RBFs)

PNN and GRNN are members of the RBFs family. The PNN is a kind of the RBF suitable for classification problems while the GRNN is a kind of the RBF that is often used for function approximation. These two networks have analogous constructions, but there is a basic distinction: the PNN makes classification where the goal variable is definite, whereas the GRNN makes regression where the goal variable is continuous.

The structure of these networks consists of four layers, an input, a hidden, a summation and an output layer (see Fig.1). The input-layer neurons do not perform any computation and merely distribute input features to all the neurons in the hidden layer. The hidden layer is fully connected to the input layer. The hidden layer units represent each training set pattern and use a radial base activation function. This layer carries out a nonlinear transformation of the input space to the hidden space; the hidden space is of high dimensionality, so transforms the nonlinear separable pattern set in linear separable output sets. In fact, neurons in the hidden layer utilize multi-dimensional kernels to estimate the probability density function (PDF) for classification.

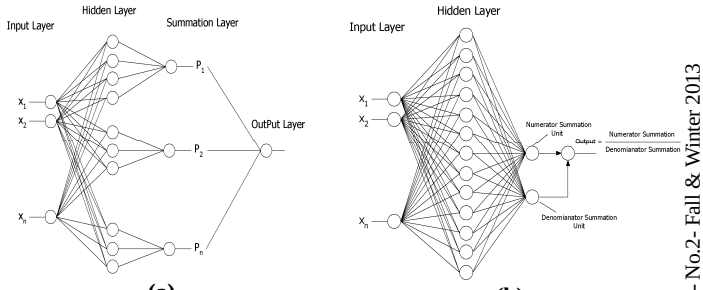

(a) (b)

Fig. 1: The neural networks structure [14]. (a) PNN. (b) GRNN.

The summation layer is different for these networks. For the PNN networks, there is one neuron for each class. This layer performs an average operation of the outputs from the hidden layer for each class. For the GRNN networks, there are two neurons in the summation layer. One neuron is the denominator summation (DS) unit; the other is the numerator summation (NS) unit. The DS unit adds together the weight values coming from every hidden neuron. The NS unit adds together the weight values multiplied by the aim value for every hidden neuron. The decision layer is different for these networks. For the PNN networks, the decision layer is a competition layer. Compete transfer function in this layer picks the maximum of these probabilities, and produces a 1 for that class and a 0 for the other classes. For the GRNN, the decision layer divides the value gathered in the NS

unit by the value in the DS unit and utilizes the consequence as the forecasted aim value [10, 14].

The basic idea behind the PNN is a direct neural network implementation, using the Parzen nonparametric PDF estimation and the Bayes strategy for pattern classification. The Parzen estimation of the PDF for class *k* is

$$pdf_k(x) = \left(\frac{1}{2\pi^{n/2}\sigma^n}\right)\left(\frac{1}{p_k}\right)\sum_{j=1}^{p_k} e^{-(x-x_{kj})^2/(2\sigma^2)} \quad (1)$$

Where x_{kj} is the *j*th training sample from class *k*, x is the unknown input, n is d the imension number of classifying vector x, p_k is the number of training sample of class *k*, and the σ is an adjustable smoothing parameter. This equation implies that the PDF for each class can be expressed simply as the sum of the population PDFs. In addition, as already mentioned, when a new input pattern x is presented to the GRNN for the prediction of the output value, each training pattern y_p assigns a membership value h_p to x, based on the Euclidean distance d_p as in (2). The distance, d_p, between the training sample and the point of prediction, is used as a measure of how well each training sample can represent the position of prediction, x. Finally, GRNN calculates the output value *y* of the pattern x as in (2) [14].

$$y(x) = \frac{\sum_{p=1}^{P} y_p \times h_p}{\sum_{p=1}^{P} h_p}, \quad h_p = \exp\left(-d_p^2 / 2\sigma^2\right), d_p^2 = (x-x_p)^T.(x-x_p) \quad (2)$$

The RBF networks have some advantages over other artificial neural networks that are presented in the following [10, 14].

•The PNN/GRNN learns instantaneously in one-pass through the patterns of the training set which causes them faster to train, compared to other networks and these networks don't need pre-decision on the number of layers and hidden units.

•The fast learning speed of the PNN makes it suitable for fault diagnosis and signal classification problems in real time (especially when implemented on hardware systems).

•There is no need to set the initial weights and no relationship exists between learning and recalling processes in these networks.

• A PNN has got an inherently parallel structure, quick repeated iterative process and superior adaptation capability for architectural changes.

•A PNN is guaranteed to converge to a Bayesian classifier, provided that it is given enough training data.

2.2. Wavelet Decomposition

Many applications use the wavelet decomposition. One of the most popular applications of the wavelet transforms is in de-noising studies on the steady state problems [11]. The aim of de-noising is to eliminate the noise and to retain the important features as much as possible. In recent times, signal de-noising studies using nonlinear processing, such as wavelet transformation, have become increasingly popular. In this project, DWT based on the filtering scheme, illustrated in Fig.2, is used for de-noising, because by reducing the noise, better network training is done. Also, with regard to simultaneously sampling data in specific angular position of the rotor, time axis has been replaced with angle axis ($(\theta_1, \theta_2, ..., \theta_{48})$).

The continuous wavelet transform (CWT) of a time-dependent signal $x(t)$ that can be defined as the sum over all time of the signal multiplied by scaled, shifted versions of the wavelet function $\psi(t)$, i.e. [12]

$$w_x(b,a) = |a|^{-\frac{1}{2}} \int_{-\infty}^{\infty} x(t)\psi^*\left(\frac{t-b}{a}\right)dt \quad (3)$$

where $\psi(t)$ is the mother wavelet, and a and b are scale index and translation parameters, respectively.

The discrete wavelet transform (DWT) is derived from the discretization of $w_x(b,a)$ and a, b can be defined as: $a = 2^j$, $b = 2^j k$, $j, k \in z$. Therefore, by using (3), the discrete wavelet transform can be expressed as following :

$$DWT(j,k) = \left|2^j\right|^{-\frac{1}{2}} \int_{-\infty}^{\infty} x(t)\psi^*\left(\frac{t-2^j k}{2^j}\right)dt \quad (4)$$

The fundamental idea of the wavelet analysis is that the original signal, $x(t)$, passes through two complementary filters and it is decomposed into approximation coefficients representing low-frequency components ($A's$) and detail coefficients representing high frequency components ($D's$).

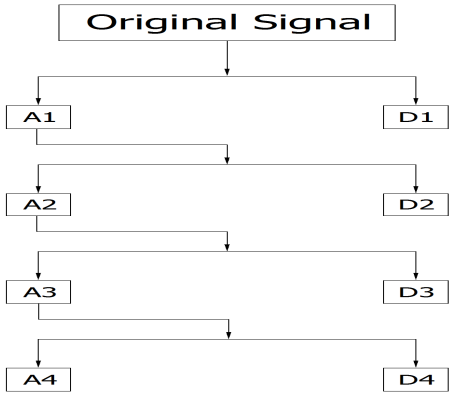

Fig. 2: Tree of four levels DWT decomposition of an original signal [12].

3. Internal Fault

3.1. Description of Internal Faults

Early stages of internal faults in stator winding may often have insignificant effects on the machine performance; however such faults may quickly lead to considerable inter-turn faults and subsequently destructive failures [15]. Undetected turn-to-turn faults lead to generated heat in the deformed region of a winding which finally develop and change into phase-to-ground or phase-to-phase faults [3]. These types of faults are a major reason of the stator winding failures and other faults may result from these faults [3]. Therefore, it is very important to analyze and detect the inter-turn winding faults. Hence, reliable and accurate diagnosis of inter-turn short circuit faults is a challenging problem in the area of fault diagnosis of electrical machines.

Fig. 3 illustrates the case when a turn-to-turn short circuit has happened in the same branch. In this figure, two currents produce opposite MMFs, one of which is the phase current and the other one is the short circuit current. The difference between these two currents is defined as circulating current I_{cir}. Therefore, the main effect of the inter-turn short circuits decreases the MMF close to the short-circuited turns. Firstly, when a short circuit occurs, the number of phase winding turns and the MMF produced by this winding reduce. Secondly, the MMF produced by the short-circuit current is contrary to the MMF produced by phase winding [1, 16]. In Fig.2, N_D corresponds to the winding turns being shorted due to turn-to-turn short circuit in the same branch and R_D corresponds to the contact resistance.

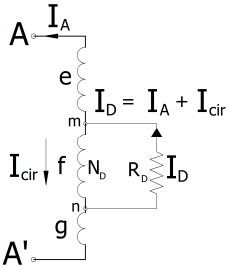

Fig. 3: Inter-turn short circuit between two points, *m* and *n* [1].

3.2. Magnetic Flux Distribution

Modeling and analysis of salient-pole synchronous generator is very complicated, especially when an inter-turn winding fault occurs in a generator equipped with a stator winding consisting of parallel branches. Fig.4 (a) and (b) shows the typical magnetic flux distribution under normal and turn-to-turn fault of the studied generator as obtained by the FEM simulation. In Fig.4 (a) magnetic flux distribution varies from 0.177 T (q-axis) to 1.503 T (d-axis). Fig.4 (b) illustrates flux distribution under turn-to-turn fault. In this figure, magnetic flux distribution varies from 0.195 T to 1.654 T. Due to the high circulating current in the fault areas; magnitude of magnetic flux linkage under fault condition in these areas is higher (also, see Fig.10). It is evident from both figures that magnetic field distribution in synchronous generator under healthy operation is symmetrical. But when a turn-to-turn fault occurs, this fault will cause nonsymmetrical distribution of magnetic flux linkage. Also, this matter will be shown in section 5 by experiments (see Figs.15-17). Therefore, magnetic field distribution could be applied for detection of the turn-to-turn faults in synchronous generator. In fact, in electrical machines, air-gap magnetic field distribution in no-load and on-load performance under healthy conditions is symmetrical (neglecting the insignificant inherent asymmetry in the magnetic field distribution due to the differences on mechanical structures). But this symmetry is specially lost under internal faults occurrence.

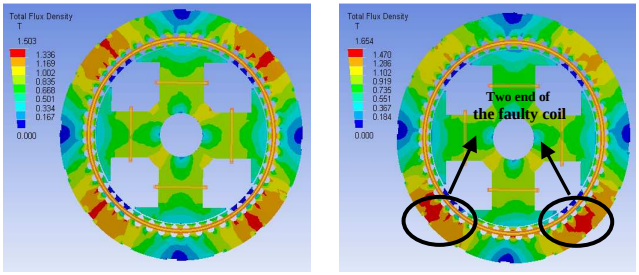

(a) **(b)**

Fig. 4: Distribution of magnetic field density in salient-pole synchronous generator (front view). (a) Under healthy condition. (b) Under turn-to-turn short circuit in stator winding.

In this research, the magnetic field distribution is calculated by 3D-FEM using ANSYS workbench software.

4. Experimental Test Setup and Measuring Technique

In this section, to demonstrate the performance of proposed method, a series of actual different kinds of inter-turn winding fault on a salient-pole synchronous generator have been fulfilled.

4.1. Experimental Test Setup

The machine used in this study is a 50 KVA, 380V, 4-pole, 1500 rpm, 50 Hz, 48 stator slots, salient-pole synchronous generator. The stator of this generator has a 3-phase, one layer, lap winding, and four parallel branches in each phase. The structure of the testing laboratory and experimental test setup is shown in Fig.5. It consists of a synchronous generator connected to a three-phase load. This generator has no damper winding, and is driven by an induction machine. In fact, a usual commercially accessible generator was

disassembled and in order to produce turn-to-turn fault, isolation of the few turns from the same coil was harmed, i.e., scratched. At these points, some conductors were soldered and taken out of the machine. Short circuit was made between these conductors. Thus, turns were shortened externally. By measuring the EMF between these conductors and having awareness of winding details, we were capable of deducing how many turns in one coil were shorted.

Also, this feature (measured EMF) can be used as a fault severity indicator. In this work, the minimum number of the stator winding turns, which are short circuited, is approximately about 5% of the total turn number.

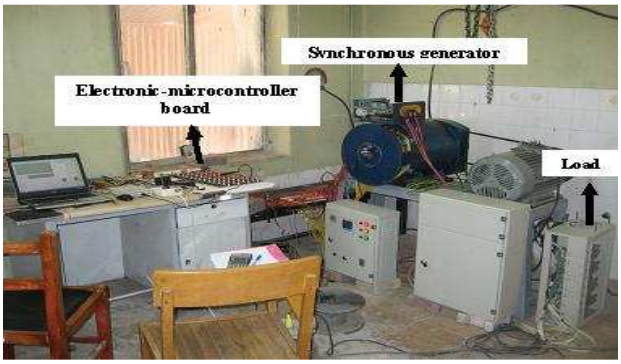

Fig. 5: Testing laboratory and experimental test setup.

A no-load experiment and a three-phase symmetrical terminal short-circuit experiment are accomplished on the machine without internal faults. Next, under low excitation condition, several of the internal faults were performed on the mentioned generator under different conditions. In these experiments, any resistor to limit the currents is not used. Also, in order to prevent severe damage to the generator, the duration of the inter-turn short circuit was limited by using a switch. However, because of the major concern over testing machine health for further tests, measurements at full excitation current were not carried out.

Through the experiments performed in this work, search coils and designed electronic-microcontroller board are used for measuring the flux linkage from inside the machine. Designed electronic-microcontroller board has one master and forty eight slaves. Electric diagram of the board is shown in Fig. 6, where two slaves (of 48 slaves) of this system can be observed. Two-wire serial interface is used in this system.

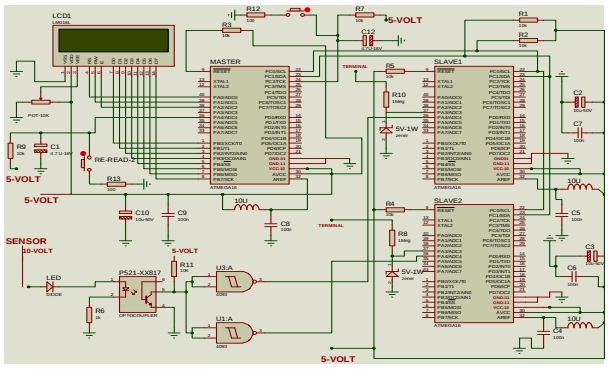

Fig. 6: Electric diagram of the designed electronic-microcontroller board for measuring the flux linkage from inside the machine.

Forty eight single turn search coils were installed along the grooves of the stator teeth with a pitch of 15° with the aim of being able to determine how the flux linkage distribution in the generator changes when an abnormal operational condition is present. The induced voltage detected by a search coil is directly proportional to the rate of change of the magnetic flux linkage [17]. Schematic and experiment view of these used search coils are illustrated in Fig.7.

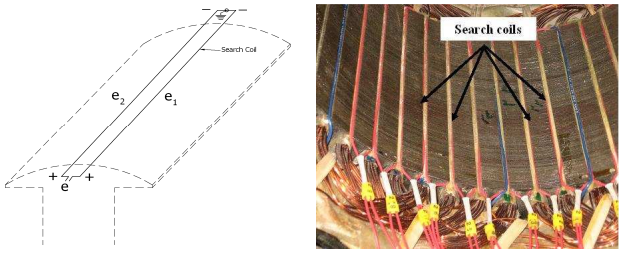

(a) **(b)**

Fig.7: (a) Schematic view of search coil. (b) Search coils placed along the stator teeth in experiment.

In other words, electronic-microcontroller board has been designed for measuring simultaneously flux data from the forty eight search coils in cross-section of mentioned generator. Serial port interface has been used for connecting designed electronic-microcontroller board to computer. The induced voltages in the search coils are communicated to serial port of the computer by means of designed electronic-microcontroller board. This structure is shown in Figs.5 and 8.

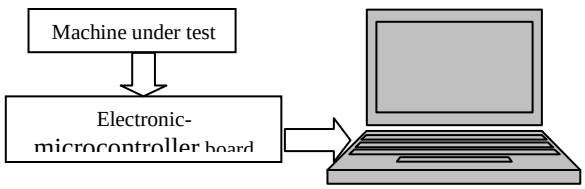

Fig. 8: Waveform samples are transferred to a standard personal computer (PC).

4.2. Induced Voltage in Search Coils under Healthy and Faulty Operations

Figs. 9 and 10 show the measured voltage induced in 31st search coil, under healthy and faulty operations at no-load respectively. Under faulty operation, induced voltage in search coil is distorted.

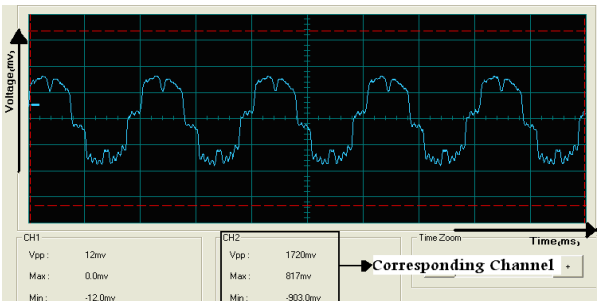

Fig. 9: Measured voltage under healthy operation (no-load).

Although influence of load level on the detection procedure might seem a drawback, experimental tests showed it is possible to make a reliable diagnosis. Fig.11 shows induced voltages in 31st search coil, under different on-load conditions in the normal and faulty operations. Due to limitation in the power of the induction machine, generator has been loaded up to a maximum of around 25% of the rated load.

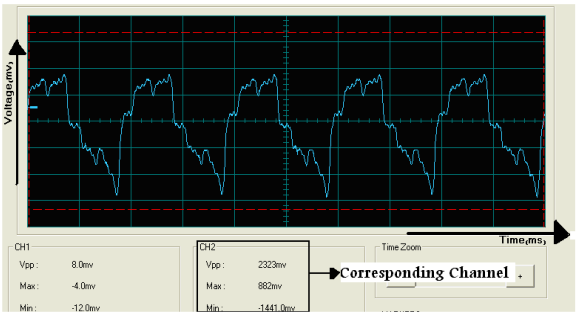

Fig. 10: Measured voltage under faulty operation (no-load).

As it is seen in this figure, the generator load level does not have a major influence on the performance levels of the method. According to Figs.9, 10, and 11, due to the effect of the armature reaction, under on-load conditions, the induced voltages in the search coils slightly deviate from the induced voltages in the search coils under no-load conditions. In fact, in a p poles, healthy, symmetrical machine, the magnetic axis of each pole is located at 360/p geometrical degrees [18]. Under load conditions, the pole axis is not an axis of symmetry whereas in no-load conditions the pole axis is axis of symmetry. When a generator is delivering power to the load, the axes of symmetry of the magnetic field deviates from the polar and interpolar axes [19]. It is obvious that, this condition (resistive load) gives maximum deviation [20].

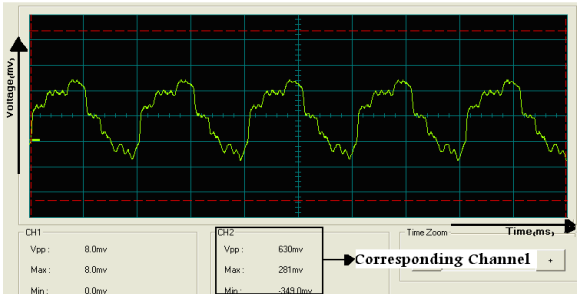

(a) Load level= 7% -Under healthy operation.

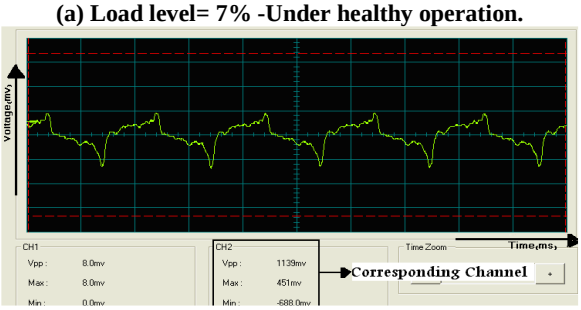

(b) Load level= 7% - Under faulty operation.

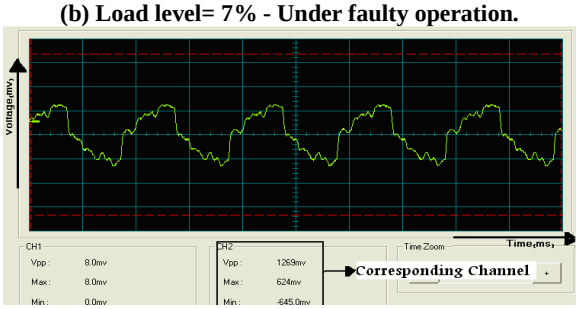

(c) Load level= 13% -Under healthy operation.

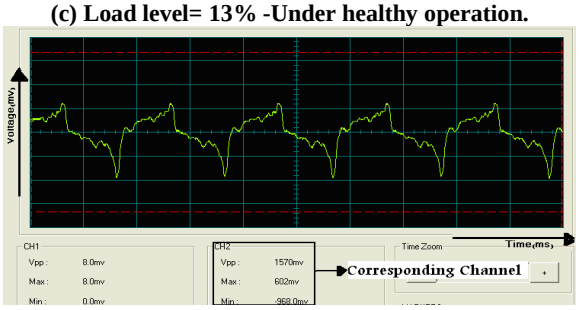

(d) Load level= 13% - Under faulty operation.

Fig.11: Induced voltage in the 31st search coil under different on-load conditions in the normal and faulty operations.

5. Finding Fault Signatures

As far as the authors are aware, most of the presented techniques do not offer the capability of identifying the specific faulty coil [21-28]. On the other hand, as discussed in [29], in lap winding machine not only faulty coil can not detected, but also finding the faulty phase is too difficult. In lap wound machines, the electrical space phase shift between the magnetic axis of the faulty coil and the original magnetic axis of the phase winding depends on the location of the shorted coil, the number of coils per phase and the distribution of the coils in the stator slots. Consequently, it is

difficult to detect the faulty phase in these types of machines [29]. In addition, finding a clear fault signatures in a machine equipped with the stator winding configurations of the parallel branches in internal faults is a difficult task [1]. On the other hand, along with the growth of electric power industry, investigation of fault diagnosis of synchronous generators with several parallel paths becomes more and more significant [21].

Although the stator of studied generator in this paper has lap winding and four parallel branches in each phase, the proposed technique with the aid of neural network could identify the faulty phase and coils under inter turn winding faults. As representative examples of the many tests performed on the salient-pole synchronous generator in the laboratory, one illustration for each case is presented.

In the following subsection (1 & 2), procedure for finding a clear fault signatures based on two schemes is presented. Under the first, detection of faulty phase based on space analysis of induced voltage in search coils is presented. In the second, detection of faulty coil based on time analysis of induced voltage in search coils is presented.

5.1. Finding Fault Signatures Based on Space Analysis of Induced Voltage in Search Coils

The detailed data of the two experiment tests of the shorted turns in phase *B* and *C* are listed in Table I. These data are sampled simultaneously from the forty eight search coils by the electronic-microcontroller board in specific angular position of the rotor that is given in Fig.12 ($\theta = 0$). Winding arrangement and geometry of this generator are shown in Fig.12.

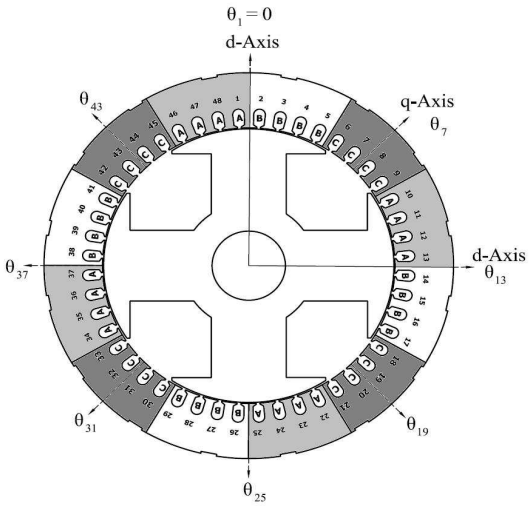

Fig.12: Winding arrangement and geometry of salient-pole synchronous generator.

In Table I, No. is the number of the search coils and values of sampled voltages under normal and faulty operations (induced in four adjacent search coils of each phase) which have been collected together (presented by *S.N* and *S.F*). The absolute values of the difference between the normal (*S.N*) and fault (*S.F*) values are presented by *DIF*.

Table 1:
Sampled voltages due to the experiment tests of the shorted turns in phase "b" and phase "c" (volt)

	Turn-to-turn short circuit at two branches in phase V Excitation Current= 2.1 A					Turn-to-turn short circuit at the same branch in phase W- case 1 Excitation Current= 3 A				
No	*N*	*F*	*S.N*	*S.F*	*DIF*	*N*	*F*	*S.N*	*S.F*	*DIF*
2	0.83	1.08	3.01	4.22	1.21	1.14	1.13	3.89	3.73	0.16
3	0.79	1				1.05	1			
4	0.74	1.19				0.9	0.9			
5	0.65	0.95				0.8	0.7			
6	0.06	0.09	-0.41	-0.26	0.15	0.06	0.07	-0.58	-0.52	0.06
7	0.05	0.08				0.05	0.08			
8	-0.06	-0.07				-0.12	-0.13			
9	-0.46	-0.36				-0.57	-0.54			
10	-0.68	-0.55	-3.27	-3.28	0.01	-0.8	-0.72	-3.82	-3.71	0.11
11	-0.83	-0.75				-0.9	-0.88			
12	-0.81	-0.88				-1	-1.06			
13	-0.95	-1.1				-1.12	-1.05			
14	-0.86	-1.2	-3.24	-4.45	1.21	-0.98	-0.97	-3.8	-3.87	0.07
15	-0.84	-1.4				-1.09	-1.11			
16	-0.84	-1.1				-0.95	-0.96			
17	-0.7	-0.75				-0.78	-0.83			
18	-0.04	0.02	0.59	0.66	0.07	-0.4	-0.35	0.44	0.22	0.22
19	-0.01	-0.07				0.02	-0.01			
20	0.09	0.17				0.21	0.06			
21	0.55	0.54				0.61	0.52			
22	0.58	0.63	2.97	3.25	0.28	0.73	0.5	4.05	2.9	1.15
23	0.74	0.76				0.93	0.6			
24	0.8	0.85				1.29	0.95			
25	0.85	1.01				1.1	0.85			
26	0.8	1.3	2.87	4.11	1.24	1.05	1	3.73	2.75	0.98
27	0.75	1				1	0.7			
28	0.7	1.2				0.85	0.65			
29	0.62	0.61				0.83	0.4			
30	0.04	-0.08	-0.47	-0.49	0.02	0.04	-0.1	-0.66	-0.84	0.18
31	0.02	0.08				0.02	0.03			
32	-0.05	-0.06				-0.1	-0.15			
33	-0.48	-0.43				-0.62	-0.62			
34	-0.6	-0.55	-3.13	-3.4	0.27	-0.8	-0.7	-3.82	-3.66	0.16
35	-0.76	-0.85				-0.9	-0.96			
36	-0.86	-1.1				-1	-0.95			
37	-0.91	-0.9				-1.12	-1.05			
38	-0.81	-1.11	-2.86	-3.57	0.71	-0.98	-1.05	-3.8	-3.83	0.03
39	-0.76	-1				-1.09	-1.08			
40	-0.72	-0.88				-0.95	-0.85			
41	-0.57	-0.58				-0.78	-0.85			
42	-0.03	-0.13	0.58	0.49	0.09	-0.4	-0.42	0.45	0.45	0.07
43	0.09	0.08				0.06	0.09			
44	0.04	0.05				0.18	0.23			
45	0.48	0.49				0.61	0.62			
46	0.52	0.44	2.8	3.01	0.21	0.73	0.78	3.8	3.69	0.11
47	0.7	0.72				0.93	0.76			
48	0.77	0.75				1.15	1.18			
1	0.81	1.1				0.99	0.97			

Fig.13 (a) shows the experiment result of the shorted turns in two branches on the coils between the 4th and 14th slots and the 5th and 15th slots in phase *B* at 50% (tap to terminal) of branch 1 and 75% (tap to terminal) of branch2 (corresponding detailed data are presented in Table I). In this figure, the difference between the normal and fault values are presented. According to this figure, the amplitude of the difference between the normal and fault values in phase *B* is larger than that of the other phases that

indicates fault has occurred in phase *B*. Fig.13 (b) shows the experiment result of the shorted turns in two branches on the coils between the 24th and 34th slots and the 25th and 35th slots in the phase *A* at 5% (tap to terminal) of branch1 and 45% (tap to terminal) of branch2. In this figure, the difference between the normal and fault values are presented. According to this figure, the amplitude of the difference between the normal and fault values in phase *A* is larger than that of the other phases that indicates fault has occurred in phase *A*. In these two cases, the magnetic axes of the faulty coils are approximately placed under q-axis ($\text{in}\,\theta = 0$, see Fig.12) so the flux linkages between the faulty coils and the other windings will be large due to the minimum reluctance between the stator and rotor in these areas. Hence, flux linkage variations to normal condition will be large in the faulty phase.

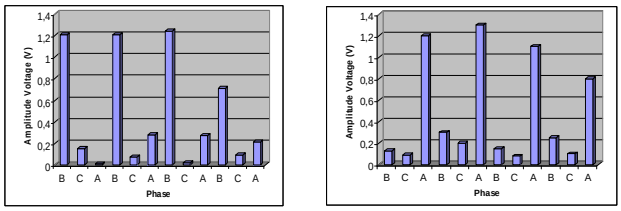

(a) **(b)**

Fig. 13: Difference induced voltage between the normal condition and faulty condition of the shorted turns in two branches in the same phase (experiment). (a) Phase *B*. (b) Phase *A*.

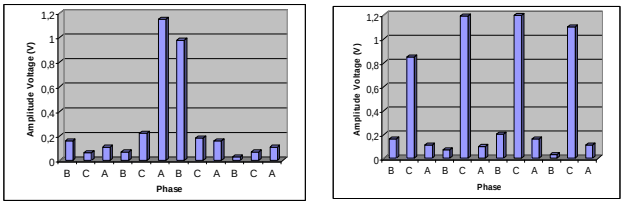

(a) **(b)**

Fig.14: Difference induced voltage between the normal condition and faulty condition of the turn-to-turn short circuit in the same branch in phase *C* (experiment). (a) Magnetic axis of the faulty coil is placed under d-axis. (b) Magnetic axis of the faulty coil is placed under q-axis.

Fig.14 (a) illustrates the experiment result in the case of turn-to-turn short circuit in the same branch on the coil between the 21st and 31st slots in phase *C* ($\text{in}\,\theta = 0$). The corresponding detailed data of this case (case1) are listed in Table I. Approximately 35% of the total turn number of the stator winding are short circuited. This figure shows that the amplitude of the difference between the normal and fault values in the area between the two slots 21 and 31 have significant changes. In this case, the magnetic axis of the faulty coil is placed under d-axis. Also, Fig.14 (b) again shows the experiment result in the case of turn-to-turn short circuit in the same branch on the coil between the 21st and 31st slots in phase C. But in this case, the position of rotor is changed in such a way that the magnetic axis of the faulty coil is placed under q-axis. This figure shows that the amplitude of the difference between the normal and fault values in phase *C* is larger than that of the other phases.

The behavior of these two faults in phase *C* can be explained as follows:

when the magnetic axis of the faulty coil is placed under d-axis (see Fig.12), the flux linkage between the faulty coil and the other windings will be small due to the large air gap between the stator and rotor in these areas. Therefore, the induced voltage in the search coils in these areas will have less variation than that of normal condition. In fact, when an inter-turn short circuit occurs, flux linkage variation is large in search coils placed under poles in the area between the two faulty slots (see Figs.12 and 14 (a)). When the magnetic axis of the faulty coil is placed under q-axis, the flux linkages between the faulty coil and the other windings will be large due to the minimum reluctance between the stator and rotor in these areas. Hence, the flux linkage variation to normal condition will be large in the faulty phase.

5.2. Finding Fault Signatures Based on Time Analysis of Induced Voltage in Search Coils

Fig.15 shows the forty eight voltage waveform (induced in the search coils) under no-load condition in the healthy operation. In this figure, symmetry in the magnetic field distribution under healthy operation is presented (also, see Fig.4 (a)).

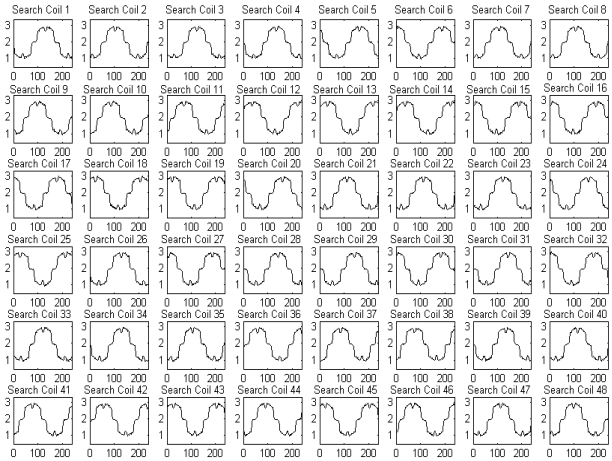

Fig.15: Forty eight measured voltage under healthy operation (no-load).

As it was mentioned earlier, under ideal conditions, the machine has an air-gap magnetic field which varies sinusoidally in space and time. Faulty operation will cause a distortion of this sinusoidal waveform. When the stator winding inter-turn fault occurs, the induced voltages in the search coils of the faulted area change more than those of the other search coils. Because

voltage difference and circulating current will occur, the flux linkage in these areas will be most affected with this fault. This concept is shown in Fig.16.

To demonstrate this concept, we have created an experimental turn-to-turn fault on the coil between the 21st and 31st slots in phase *C*, and the induced voltage in forty eight search coils has been measured. Fig.16 shows the forty eight voltage waveform under no-load condition in the faulty operation. According to this figure, the symmetry in the magnetic field distribution is lost and induced voltage in search coils around two ends of the faulty coil are distorted. Induced voltage in these search coils have more change to induced voltage in other search coils that indicates the fault has occurred in relative coils of them (also, see Fig.4 (b)).

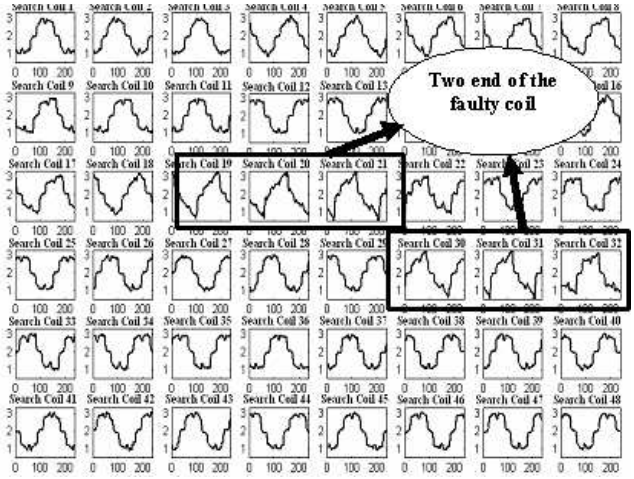

Fig.16: Forty eight measured voltage under turn-to-turn short circuit in the same branch in phase *C* (no-load).

Also, similar results were obtained from tests under turn-to-turn short circuit of two branches in the same phase. Fig.17 shows the experiment result of the shorted turns in two branches on the coils between 4th and 14th slots and 5th and 15th slots in phase *B* at 50% (tap to terminal) of branch1 and 75% (tap to terminal) of branch2. According to this figure, it is evident that the symmetry in the magnetic field distribution is lost and induced voltage in search coils around two ends of the faulty coils are distorted. In these faults, the flux linkage adjacent to the faulty coils considerably distorts.

The proposed technique can identify the occurrence of these two types of faults as well as faulted coils.

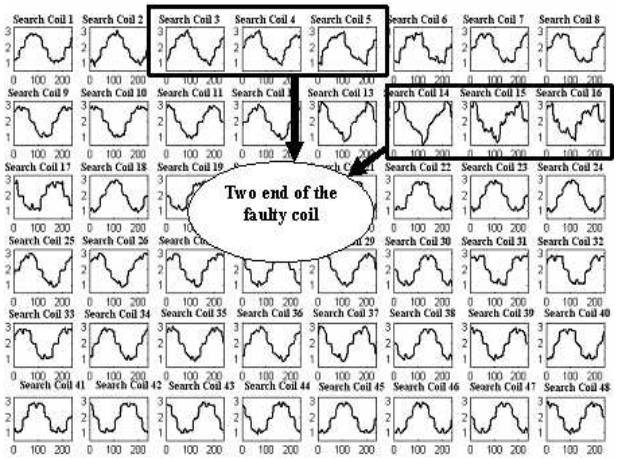

Fig.17: Forty eight measured voltage under turn-to-turn short circuit of two branches in the same phase in phase *B* (no-load).

It should be remembered that due to the effect of armature reaction under on-load conditions in the normal and faulty operations, induced voltage in the search coils slightly leave from the induced voltage in the search coils under no-load conditions (see Figs.9, 10, and 11).

6. Design of Fault Diagnosis System Using Neural Network

In our wok, the PNN, the GRNN and the DWT are used in the design of fault diagnosis system. For suitable analysis with the aid of neural networks, software with a graphical user interface has been designed in MATLAB software (see Fig.18).

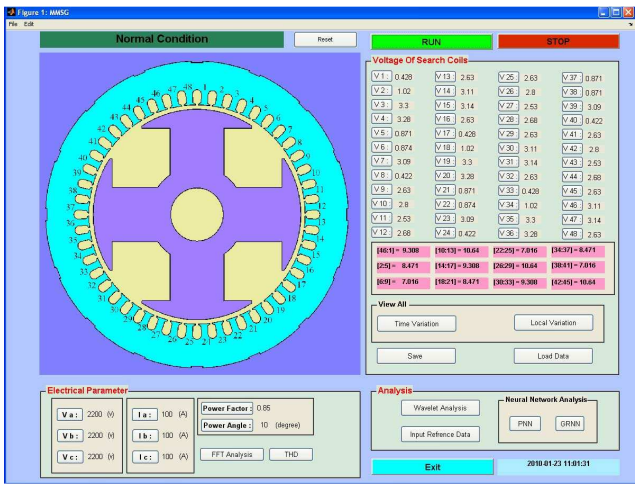

Fig.18: Graphical User Interface.

PNN as main part of this fault diagnosis system and DWT are combined effectively to construct the classifier. The PNN is trained by features extracted from the magnetic flux linkage data through the discrete meyer wavelet transform. PNN is trained with simulation data and then PNN is tested with

experimental data. In fact, similar to training section the measured slot flux linkage is preprocessed with wavelet transform and then in order to detect the fault, approximation signal at level 4 is fed to PNN. The training database for the PNN is generated by the 3D-FEM. Since the FEM simulation is a time-consuming process, in order to reduce the number of FEM computations the GRNN was used to estimate the flux linkages characteristics under various conditions.

The GRNN is used to build training database for the PNN and its aim is to estimate the flux linkage of the machine for a given set of input under healthy and faulty conditions. In fact, instead of the traditional look-up table and interpolation methods, the GRNN is used. It must be noted that, the FEM computation needs to be performed on only several key states in different coil positions. Then, these data (obtained from FEM computation) will be used as inputs for training the GRNN. After the GRNN is trained, it will be used to estimate the nonlinear flux linkage of the machine in other conditions.

On the other hand, after the GRNN is trained, the next step is to ensure its performance, that is, how it behaves to an arbitrary input which is not in the training set. In order to check this performance, diverse set of inputs are selected. These test load points (computed by FEM) are presented as inputs for training the GRNN. Then the GRNN estimates the nonlinear flux linkage in the cross-section of the machine. For instance, in two excitation current (2.1 A, 2.4 A), nonlinear flux linkages of the machine were estimated. In order to check the accuracy and validity of the GRNN-based flux linkages, the flux linkages at these test points were recomputed using the FEM technique.

Table 2:
Range of errors between the fem computed flux linkages with GRNN estimated and interpolated flux linkages

Different methods	Neural network	Different methods of interpolation			
	GRNN	Linear	Cubic spline	Piecewise cubic Hermite	Nearest neighbor
Max error	4.8%	15%	9%	13%	38%
Min error	0%	1%	0.2%	0.5%	2%

Also, flux linkages of the machine in these test points were interpolated with different methods. Then the percentage error between the FEM computed flux linkages and the GRNN was estimated and the interpolated flux linkages were calculated. Range of these errors is presented in Table II. As it can be seen the maximum error between the GRNN-based and the FEM computed flux linkage is less than 5%. This is less than the estimation error of the other methods. This demonstrates the strong ability of the GRNN in the estimation of the flux linkages once it is successfully trained.

From the previous results, we can conclude: if the parameters of the FEM-based model are available for some fault cases, the parameters for other fault cases can be easily estimated by the GRNN. In other words, the FEM computation needs to be performed on only several key states in different coil positions and other states will be estimated with the GRNN. This demonstrates the practicality of building the FEM-based model for various internal fault conditions.

6.1. Detection of Faulty Phase by MWPNN

In this subsection, procedure for detection of faulty phase by MWPNN based on the previous discussion and the experimental results in section 5.1 is presented.

When a synchronous generator is working under healthy condition, it is clear that the flux distribution should be symmetrical, neglecting the insignificant inherent asymmetry due to the differences on mechanical structures. But this inherent asymmetry in the machine used in this study is higher duo to fatigue and lack of optimal design.

Regarding the number of poles in the aforementioned generator, its cross-section was divided into four areas in our analysis. For instance, by using data from Table I and other experiment tests, absolute value of samples in each area has been collected together. These results are presented in Table III. As it is seen from Table III, in the normal operations the difference between these data is under 10%. But, when an inter-turn short circuit occurs, this flux asymmetry will be higher than the normal value. In the faulty operations the maximum difference between these data is over 10%. It must be noted that the foundation of the presented results in Table III is based on the comparison of data in all four areas. Voltage deviations are the same in these areas due to the variation of the load level. Hence, increasing or decreasing in load level does not cause major changes in these results (see Fig.11). Therefore, by the examination of different conditions, threshold value to separate normal and fault is set at 10%. It must be noted that the best threshold value for each machine can be obtained by the analysis of sampling data from normal performance of the machine in a specified period of time.

Table 3:
Summated value of sampled voltage data in four areas (volt)

Number of search coils	Turn-to-turn short circuit at two branches in phase B Load level= 16%				Turn-to-turn short circuit at the same branch in phase C- case 1 Load level= 22%			
	Normal		*Fault*		*Normal*		*Fault*	
	No-load	Load	No-load	Load	No-load	Load	No-load	Load
2-13	6.69	7.4	7.76	8.9	8.29	9.12	7.96	9.15
14-25	6.8	7.45	8.36	9.7	8.29	9.15	6.99	7.47
26-37	6.47	6.92	8	9.1	8.21	8.75	7.25	8.34
38-1	6.24	6.8	7.07	7.8	8.05	8.8	7.97	9.01
Maximum difference	8%	8.7%	16%	19.5%	2.89%	4.37%	12.3%	18.4%

So, as a result of delaminating clustering, the input data is classified step by step. Hence, based on the previous discussion, the fault class is divided into normal or fault based on the threshold value. Then, we classify the fault data in order to detect the faulty phase. This process is illustrated in Fig.19.

Magnetic flux linkage data of the stator teeth in different angle $(\theta_1, \theta_2, ..., \theta_{48})$ are used as input data for training and testing the PNN (see Fig.12). The PNN is trained by the features extracted from the magnetic flux linkage data through the discrete meyer wavelet transform (approximation signal at level 4 is fed to PNN)

.

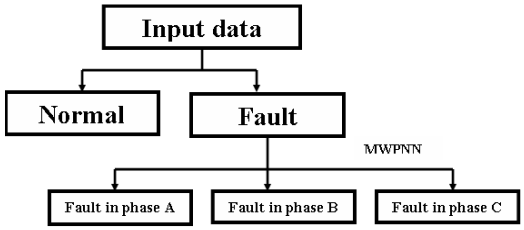

Fig. 19: Delaminating diagram for detection of faulty phase.

Table 4:
Parameters of the MWPNN for detection of the faulty phase

Method	Related parameter		
PNN	Input layer	48	nodes
	Output layer	3	nodes
	Smoothing parameter	0.5	

In order to build the flux linkage look-up table, the variation range of excitation current and short circuit turn ratio needs to be determined first. In our work, the power factor is one due to a three-phase resistive load and regarding the nameplate of the machine, the variation range of excitation current is set as 2 A to 7 A and short circuit turn ratio is set from 5% to 65%. For instance, in this work, in the case of turn-to-turn short circuit in the same branch, we use 1 A and 10% as the computational steps for the excitation current and short circuit turn ratio.

In the input training data for each coil (8 coils), the short circuit turn ratio (α) varies as follows: 5%, 15%, 25%, 35%, 45%, 55%, and 65%. Corresponding to each short circuit turn ratio, the excitation current, the load current, and the fault current have different values. Computational steps for the excitation current are considered as follows: 2, 3, 4, 5, 6, and 7 A. For each excitation current, the load current, and the fault current are calculated in corresponding short circuit turn ratio with the equations described in section II. So, totally 336 cases that $192=8(\text{coil})\times 4(\alpha)\times 6(\text{excitation current})$ cases computed by the 3D-FEM and $8\times 3\times 6=144$ cases estimated by the GRNN are considered to build the flux table for each phase. Therefore, 336×3(number of phases) =1008 sets of input-output are used to train the PNN to detect the faulty phase (each 336 cases represent one phase). The input data used in this method are the steady state data. It must be noted that concerning practical load point, the variation range of variables can be limited. Hence, computations will be reduced. On the other hand, the small computational steps will improve the accuracy of the detection. Table IV lists the parameters of the MWPNN in this procedure for detection of faulty phase.

6.2. Detection of Faulty Coil by MWPNN

In this subsection, procedure for detection of faulty coil by PNN and DWT, based on the previous discussion and the experimental results in section 5.2 is presented. Forty eight search coils are sampled simultaneously in one or more cycles (depending on the used hardware). Therefore, a vector sets are obtained. The obtained waveforms are analyzed by wavelet transform and de-noised signals are extracted. Then PNN is trained by features extracted from the magnetic flux linkage data through the discrete meyer wavelet transform (approximation signal at level 4 is fed to PNN).

In this scheme, regarding the number of search coils; forty eight MWPNN is used for detection of faulty coils. Each MWPNN is carried out only for two classes i.e., normal and fault for the classification. When no faults are present in the generator, all MWPNN's will predict the normal class. If some MWPNN's predict the fault class, the turn-to-turn short circuit in the same branch or turn-to-turn short circuit of two branches in the same phase has occurred. This process is illustrated in Fig.20.

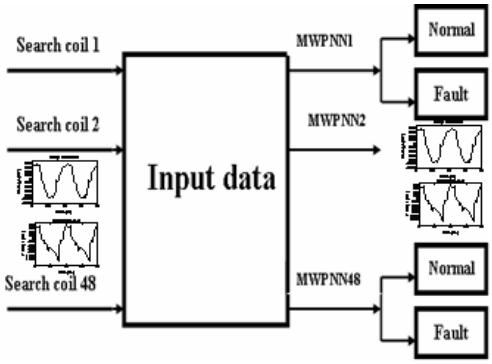

Fig. 20: Procedure for detection of faulty coil by MWPNN.

Each neural network is trained with 5 input data (or events) of each class. Table V lists the parameters of the MWPNN in this procedure for detection of faulty coil.

Table 5:
Parameters of the MWPNN for detection of the faulty coil

Method	Related parameter		
PNN	Input layer	240	nodes (depending on the used hardware)
	Output layer	2	nodes
	Smoothing parameter	0.5	

7. Evaluation of Performance

The influence of different kinds of mother wavelets to the classification accuracy was also investigated. It will provide the evidences for choosing proper wavelet family. Five commonly used wavelets, named Meyer wavelet, Haar wavelet, Daubechie's wavelet, Symmlets and Coiflets wavelet are considered. In order to evaluate the performance of different kind of mother wavelets, we choose the same decomposition level up to 6 levels. The highest classification accuracy is obtained with meyer wavelet in level 4. Hence in order to detection the fault, discrete meyer wavelet transform is used and approximation signal at level 4 is fed to PNN.

Therefore, meyer wavelet probabilistic neural network (MWPNN) is used as supervised classifier. In design of the MWPNN, it is very important to select an optimal value of the smoothing parameter. Procedure of classifying starts with finding the optimal smoothing value for MWPNN. The traditional trial and error method is used to obtain optimum smoothing factor. The second step of the classifying process is to find a good training set. Cure must be taken in choosing data for obtaining a good training set in order to increase the performance of a neural network. The smoothing parameter is given by (5) [7].

$$\sigma_i = g d^i_{j_{avg}} \qquad (5)$$

where d^i_j denotes the distance between the jth sample and nearest neighbor sample in class i and g is a constant value that has been found experimentally.

To evaluate the performance of MWPNN, its results are compared with different artificial neural networks. These different networks are trained and subsequently tested with same data due to similar procedure that has been mentioned before. These data for training are obtained from computation with FEM and estimated by GRNN. Then ANNs are tested with experimental data. These simultaneously data are sampled with designed electronic-microcontroller board from the forty eight search coils in cross-section of mentioned generator. First fault diagnosis system uses BP neural network. Second system uses PNN and third system uses MWPNN.

Table 7:
Diagnosis accuracy for test results

ANN	MLP	PNN	MWPNN
Classification accuracy	45%	70%	95%

It must be noted that backpropagation neural network is most widespread among all artificial neural networks. These networks are also make reference to as multilayered perceptron (MLP) or feedforward networks. The multilayered perceptron neural network is trained with the Batch Gradient Descent with Momentum. In detection of faulty phase, for the MLP neural network, several network configurations were tried, and better results have been obtained by a network constituted by three layers with 48, 24, and 3 neurons. Sigmoid is selected as the act function of neurons in every layer. The results of comparison for detection of faulty phase are presented in Table VI.

Table 6:
Diagnosis accuracy for test results

ANN	MLP	PNN	MWPNN
Classification accuracy	55%	78%	>95%

Also, in detection of faulty coil, for the MLP neural network, several network configurations were tried, and better results have been obtained by a network constituted by three layers with 240, 24, and 2 neurons. Sigmoid is selected as the act function of neurons in every layer. The results of comparison for detection of faulty coil are presented in Table VII.

8. Conclusion

This paper studied the use of radial basis neural networks to detect and locate an internal short circuit on the stator windings of the synchronous generator. The idea was to use data provided by precise FEM simulations of generator operation under different conditions to create identification based artificial neural network model which can be used for fault detection. In fact proposed method uses samples of magnetic flux linkages to reach a decision. The successful achieved results show that this technique is effective to ensure a reliable and accurate fault diagnosis process.

Acknowledgment

This work is supported by the Mashhad Power Station. The authors are appreciative to Mr.Borzoe for his assistance. Authors wish to thank Mr. Dehnavi, Dr. Hashemian and Mr. Pordeli in providing the experimental test setup and testing laboratory.

References

[1] M.D.Negrea, “Electromagnetic flux monitoring for detecting faults in electrical machines,” Ph.D.dissertation, Helsinki University of Technology, Laboratory of Electromechanics, Helsinki, Finland, 2007. The dissertation can be read at http://lib.tkk.fi/Diss/isbn9512284774.

[2] M. Joorabian, S.M.A. Taleghani, and R.K. Aggarwal , “Accurate fault locator for EHV transmission lines based on radial basis function neural networks,” Electric Power Systems Research, Elsevier 71,pp. 195–202, May.2004.

[3] S. Nandi, H.A.Toliyat, and X.Li, “Condition monitoring and fault diagnosis of electrical machines-A Review,” *IEEE Trans. Energy Convers.*, vol. 20, no. 4, pp. 719–729, Dec.2005.

[4] G.K. Singh, and S.A.S Al Kazzaz, “Induction machine drive condition monitoring and diagnostic research-a survey,” Electric Power Systems Research, Elsevier 64 (2), pp. 145–158, Feb.2003.

[5] M.Tripathy, R.P.Maheshwari and H.K.Verma, “Probabilistic neural network based protection of power transformer,” *IET Electr. Power Appl.*, vol. 1, no. 5, pp.793-798, Sep.2007.

[6] S. Mishra, C. N. Bhende, and B. K. Panigrahi,, “Detection and classification of power quality disturbances using s-transform and probabilistic neural network,” *IEEE Trans. Power Del.*, vol.23, no. 1, pp. 280–287, Jan. 2008.

[7] W. H. Tang, J. Y. Goulermas, Q. H.Wu, Z. J. Richardson, and J. Fitch, “A probabilistic classifier for transformer dissolved gas analysis with a particle swarm optimizer,” *IEEE Trans. Power Del.*, vol.23, no. 2, pp. 751–759, Apr. 2008.

[8] علیرضا رضائی، ابوالقاسم اسدالله راعی، ابولفضل نادی، سعید شیری قیداری "بهبود یادگیری رفتار روبات سیار دارای خطا در سنسورهای آن با استفاده از شبکه بیزین "مجله انجمن مهندسین برق و الکترونیک ایران، سال هشتم، شماره اول، بهار و تابستان ۱۳۹۰.

[9] امید قادری، محمد رضا فیضی "ارائه یک سیستم ترکیبی جدید در تشخیص نوع خطا در ترانسفورماتورهای قدرت بر اساس مقادیر گازهای حل شده در روغن "مجله انجمن مهندسین برق و الکترونیک ایران، سال هشتم، شماره اول، بهار و تابستان ۱۳۹۰.

[10] D.Gerbec, S.Gasperic, I.Smon, and F.Gubina ,“ Allocation of the load profiles to consumers using probabilistic neural networks,” *IEEE Trans.Power Systems*, vol. 20, no. 2, May 2005.

[11] W.B.Hu, K.C.Li, D.J.Zhao, and B.R.Xie ,“Performance improvement of power quality disturbance classification based on a new de-noising technique,” *IEEE*, Proceedings of the 2007 International Conference on Electrical Machines and Systems, Seoul, Korea, 8-11 Oct. 2007.

[12] فرشته پورآهنگریان، آزاده کیانی، علی کرمی، بهمن زنج "طراحی یک سیستم هوشمند مبتنی بر شبکه های عصبی و ویولت برای تشخیص آریتمی های قلب"مجله انجمن مهندسین برق و الکترونیک ایران، سال نهم، شماره اول، بهار و تابستان۱۳۹۱.

[13] G.C.Stone, E.A.Boulter, I.Culbert, and H.Dhirani, “Electrical insulation for rotating machines,” John Wiley & Sons Publishers, pp.12–20, ISBN: 0-471-44506-1, 2004.

[14] P.Picton, “Neural Networks,” Palgrave Macmillan Publisher, pp.102–109, ISBN: 9780333948996, 2000.

[15] B.Mirafzal, R.J. Povinelli, and N.A.O.Demerdash, “Inter-turn fault diagnosis in induction motors using the pendulous oscillation phenomenon,” *IEEE Trans. Energy Convers.*, vol. 21, no.4, pp.871-882, Dec.2006.

[16] G.M.Joksimovic and J.Penman, “The detection of inter-turn short circuits in the stator windings of operating motors,” *IEEE Trans. Ind. Electron*., vol. 47 , no.5 , pp. 1078-1084,2000.

[17] J.Lenz and A.S. Edelstein, “Magnetic Sensors and Their Applications,” *IEEE Sensors Journal*, vol. 6, no. 3, pp.631-649, Jun.2006.

[18] M. F. Cabanas et al., “A new on-line method for the early detection of broken rotor bars in asynchronous motors working under arbitrary load conditions,” *Industry Applications Conference, Fourtieth IAS Annual Meeting*, vol. 1, pp.662 – 669, Oct. 2005.

[19] M.V.K. Chari,“ Nonlinear finite element solution of electrical machines under no-load and full-load conditions,” *IEEE Trans. Magn.*, vol. 10, no. 3, pp. 686–689, Sep. 1974.

[20] A.E. Fitzgerald, C.Kingsley, and S.D.Umans, “Electric Machinery,” Sixth Edition, Mc Graw- Hill.

[21] A.I.Megahed and O.P.Malik, “Simulation of internal fault in synchronous machines,” *IEEE Trans. Energy Convers.*, vol. 14, no.4, pp.1306-1311, Dec.1999.

[22] X.Tu, L.A.Dessaint, M.E.Kahel, and A.O.Barry ,“A new model of synchronous machine internal faults based on winding distribution,” *IEEE Trans. Ind. Electron*., vol. 53, no. 6, pp.1818-1828, Dec.2006

[23] V. A. Kinitsky, “Calculation of internal fault currents in synchronous machine,” *IEEE Trans. Power App. Syst.*, vol. 84, no. 5, pp. 381–389, May 1965.

[24] O.Bei, W.Xiangheng, S.Yuguang, W.Weijian and W.Weihong, “Research on the internal faults of the salient-pole synchronous machine,” *IEEE, Power Electronics and Motion Control Conference, Proceedings. PIEMC 2000. The Third International*, pp.558-563, 2000.

[25] X.Lin, Q.Tian, Y.Gao, and P.Liu**, “**Studies on the internal fault simulations of a high-voltage cable-wound generator,” *IEEE Trans. Energy Convers.*, vol. 22, no. 2, pp. 240–249, Jun.2007.

[26] X. H. Wang, Y. G. Sun, B. Ouyang, W. J. Wang, Z. Q. Zhu, and D. Howe, “Transient behaviour of salient-pole synchronous machine with internal stator winding faults,” *Proc. Inst. Electr. Eng.—Electr. Power Appl.*, vol. 149, no. 2, pp. 143–151, Mar. 2002.

[27] P.Reichmeider, D.Querrey, C.A.Gross, A.Novosel, and S.Salon ,“Partitioning of synchronous machine windings for internal fault analysis,” *IEEE Trans. Energy Convers.*, vol. 15, no. 4, pp.372-379, Dec.2000.

[28] M.Rahnama, and J.Nazarzadeh, “Synchronous machine modeling and analysis for internal faults detection,” *Electric Machines & Drives Conference, 2007. IEMDC '07. IEEE International.*

[29] A.S.Ahmed, C.C.Yeh, N.A.O.Demerdash and B.Mirafzal, "Analysis of stator winding inter-turn short-circuit faults in induction machines for identification of the faulty phase," *IEEE, Industry Applications Conference, 2006. 41st IAS Annual Meeting*, vol. 3, pp.1519 - 1524, Oct. 2006.